Manuscript submitted to *Cement and Concrete Composites*

Tailored setting times with high compressive strengths in bassanite calcium sulfoaluminate eco-cements

M. García-Maté[1], D. Londono-Zuluaga[1], A.G. De la Torre[1], E.R. Losilla[1], A. Cabeza[1], M. A. G. Aranda[1,2] and I. Santacruz[*,1]

[1] Departamento de Química Inorgánica, Cristalografía y Mineralogía, Universidad de Málaga, 29071-Málaga, Spain

[2] CELLS-Alba synchrotron, Carretera BP 1413, Km. 3.3, E-08290 Cerdanyola, Barcelona, Spain

Abstract

This work deals with the hydration of a calcium sulfoaluminate (CSA) eco-cement prepared with bassanite and different additives (type and content) at a fixed water/CSA ratio of 0.5. Pastes prepared with bassanite show high water demands, high viscosity values and short initial setting times which are related to the fast dissolution rate of bassanite and the subsequent precipitation of gypsum. These facts have a dramatic effect onto the mechanical strength values, and make necessary the addition of additives.

Here, the addition of different amounts of specific retarders (polycarboxylate, tartaric acid and phosphonic acid) not only improved the workability of pastes and mortars, but also delayed the setting time, by modifying the dissolution rates of the phase(s), and improved mechanical strengths. Finally, mortars with high compressive strengths (46 and 84 MPa at 1 and 7 days of hydration, respectively) and, chiefly, tailored setting times with high strengths have been prepared.

Keywords: X-Ray Diffraction analysis, Hydration, Compressive Strength, Sulfoaluminate.

[*] Corresponding author. Tel.: +34952131992; fax: +34952131870. *E-mail:* isantacruz@uma.es

1. Introduction

Calcium sulfoaluminate (CSA) cements are obtaining increasing attention because, in their fabrication, they release lower amounts of CO_2 (up to 40% less) than ordinary Portland cement (OPC) [1,2,3,4,5]; because of that, they are considered as eco-cements. This reduction of emissions depends on the CSA composition. Although CSA can show different compositions, they always contain more than 50 wt% of ye´elimite (also named as Klein's salt or tetracalcium trialuminate sulfate ($C_4A_3\underline{S}$)) [5,6]. Cement nomenclature will be used hereafter: C=CaO, S=SiO_2, A=Al_2O_3, F=Fe_2O_3, $\underline{S}$=SO_3, M=MgO, T=TiO_2 and H=H_2O. In addition, other phases, such as C_2S, CA, C_4AF, $C\underline{S}H_2$, $C\underline{S}H_{0.5}$, $C\underline{S}$, and so on, may also be present in their composition [7]. The main performances of these eco-cements are high early strength, fast setting time, good chemical resistance and, depending on the amount of the added sulfate, these cements can also be used as constituents of self-leveling materials [8,9,10,11]. Three steps take place during the hydration of cement pastes: the dissolution of anhydrous phases, the precipitation of new phases, and the consumption of free water.

In the case of CSA, both ye´elimite and sulfate source (for instance bassanite, $C\underline{S}H_{0.5}$) are dissolved and consequently, ettringite ($C_6A\underline{S}_3H_{32}$, also called AFt) and amorphous aluminum hydroxide (amorphous-AH_3) are formed, according to Eq. 1. The quantity of precipitated ettringite at early ages depends on the solubility of the calcium sulfate (gypsum, anhydrite or bassanite) [9,10,11,12,13]. Hence, the selection of the sulfate source (type and amount) is a key point to achieve the desired properties, mainly at early ages [9,12,13]. Bassanite ($C\underline{S}H_{0.5}$) in contact with water suffers from an intergranular attack with the consequent increasing of its surface area and hence, its water demand. In addition, a primary gypsum precipitation usually happens [12], according to Eq. 2. Both facts will increase the viscosity of the paste, and the latter will also strongly reduce the initial setting time. Thus, it will have dramatic effects onto the mechanical properties.

$C_4A_3\underline{S} + 2C\underline{S}H_{0.5} + 37H \rightarrow C_6A\underline{S}_3H_{32} + 2\,AH_3\text{-gel}$ Eq.

(1)

$C\underline{S}H_{0.5} + 1.5H \rightarrow C\underline{S}H_2$ Eq. (2)

However, the addition of selected additives (retarders and/or specific superplasticizers) may well slow down the reactions and improve the workability [12]. Retarders are usually added for that, but some superplasticizers, such as polycarboxylates, also delay the setting time [14]. The addition of a very small amount of polycarboxylate (0.02 wt%) demonstrated to improve the workability/flowability of a CSA paste prepared with bassanite without a substantial delay of the setting time, producing heterogeneous mortars with poor compressive strengths [12]. Thus it is essential to add the right amount (and type) of additive to retard the setting time, reduce viscosity and hence improve the performances of the corresponding cements and mortars.

Carboxylic acids, salts of lignosulfonic acid, carbohydrates and sodium gluconates are commonly used as set retarders in the cement hydration. Many of these compounds can be also found in water-reducer formulations (superplasticizers) [15]. Citric acid, tartaric acid, salt of phosphono alkyl carboxylic acids, malic acid [16] and some phosphorous compounds such as nitrilotris(methylene)triphosphonate can be used for more specialized applications [15], such as retarders for CSA eco-cements [16]. Retarders can be prepared as both admixtures to be added to the cement, or in the cementitious formulation.

The retarder mechanism [15,17] is thought to be mainly related to: (i) surface adsorption of retarders onto the anhydrous particle surfaces; (ii) calcium-complexation that prevents the precipitation of some phases; (iii) formation of a semi-permeable layer that will collapse by osmotic pressure gradients.

The second and third mechanisms are now generally considered unlikely: the former because very strong chelaters can be moderate retarders [18] and the latter due to direct SEM observations [19]. Thus, the first mechanism is the widest accepted. For example, Bishop and Barron [20] proposed the mechanism of “dissolution–precipitation” for phosphonic acids as an special case of the first mechanism (surface adsorption of retarders directly onto anhydrous surface), and consists of two

steps: i) dissolution (calcium is extracted from the surface of the cement grains and then the aluminum-rich surface is exposed), and ii) precipitation (the soluble calcium phosphonate oligomerizes on the particle surface or in the solution and, in the former, it will inhibit/retard further hydration).

Superplasticizers are also adsorbed onto the surface of the cement particles, including CSA based eco-cements [21], promoting the dispersion of the particles due to electrostatic, steric or electrosteric repulsions [22,23,24]. Some studies [25,26] showed that sulfate is also adsorbed onto the surface of the clinker grains, in competition to the adsorption of the superplasticizer. This behavior strongly depends on the amount of both calcium and sulfate in contact with the hydrating aluminate phase, as well as their structure [27,28]. The effectiveness of superplasticizers depends on different parameters [22], such as the properties of the materials (surface, size and type of both cement particles and additives), the amount of added additive, and the preparation of the paste (order of addition, temperature and time passed since end of mixing). Thus, the addition of superplasticizers also modifies the setting time, viscosity, thermal stability, and will definitely affect the strength development, and durability of mortars and concrete [29].

This work is part of a deep study on CSA eco-cements. The amount of the sulfate source was previously optimized elsewhere [30] through phase assemblage and mechanical strenght measurements, and also the effect of different sulfate sources [12] was studied. Due to the short setting time of bassanite-pastes the hydration and performances of the corresponding pastes and mortars are expected to be controlled/improved through the addition of additives. Thus, the objective of this work is to control the hydration, including setting time, of a CSA cement paste prepared with 25 wt% of bassanite at a water/cement ratio of 0.5 through the addition of different additives (type and content). This study includes the characterization of the first hours of hydration through rheology, setting time determination, impedance spectroscopy, temperature evolution and in-situ laboratory X-ray diffraction. Moreover, the phase assemblage of cement pastes at 1 and 7

days of hydration has been determined and correlated to the compressive strengths of the corresponding mortars.

2. Materials and methods

2.1. Materials

2.1.1. Preparation of anhydrous cements

CSA clinker (industrially produced in China) and commercial micron-sized natural gypsum ($C\underline{S}H_2$) both marketed by BELITH S.P.R.L. (Belgium) were used as raw materials. Bassanite ($C\underline{S}H_{0.5}$) was prepared by heating the as received gypsum at 90ºC for 48 h. Calcium sulfoaluminate cements were prepared by mixing CSA clinker with 25 wt% of bassanite. The elemental analyses of both commercial raw materials (CSA clinker and gypsum) determined by X-ray fluorescence (XRF) are provided as supplementary information (Table S1). Blaine fineness values of CSA, gypsum and bassanite are 3497±25, 2600±51 and 2877±69 cm^2/g, respectively.

2.1.2. Cement paste preparation.

Cement pastes were prepared with distilled water at a water/cement (w/c) mass ratio of 0.5. Different amounts (from 0 to 0.45 wt% of active mater referred to cement content) of three additives were added to water (prior to the addition of the cement) for a better comparison: i) a commercial polycarboxilate-based superplasticizer, Floadis 1623 (Adex Polymer S.L., Madrid, Spain), with 25 wt% of active matter, labeled as PC; ii) tartaric acid (Adex Polymer S.L., Madrid, Spain), named TA hereafter; and iii) nitrilotris(methylene)phosphonic acid (Sigma-Aldrich), labeled as PA. PC is generally used as superplasticizer (although the used polycarboxylate also retards the hydration), and TA and PA as retarders.

Pastes with the selected amount of each additive, and also without additives for the sake of comparison, were prepared in an agate mortar and poured into a hermetically closed polytetrafluoroethylene (PTFE) cylinder shape mold [12] with 2.8 $cm^3$of volume and rotated, during

the first 24 h, at 15 rpm at 20±1ºC. This was performed to fully assure the homogeneity of the pastes during the first hours of hydration. Then, samples were taken out and stored within distilled water at 20±1ºC until further characterization.

2.1.3. Stopping cement hydration.

The as-prepared cement pastes were milled into fine powder in an agate mortar at 1 and 7 days of hydration, and then the hydration was stopped. For that, the powder was washed twice with acetone (Prolabo S.A.) and once with diethyl ether (Prolabo S.A.) in a Whatman system (70 mm diameter Whatman filter with a pore size of 2.5 μm and a Teflon support) [12,31,32]. The obtained powder was kept into a desiccator to avoid any hydration or carbonation.

2.2. Characterization.

2.2.1. Rheological behavior.

Pastes for rheological characterization were prepared by mechanical stirring with helices according to EN196-3:2005 standard procedure. A viscometer (Model VT550, Thermo Haake, Karlsruhe, Germany) with a serrated coaxial cylinder sensor, SV2P, provided with a solvent trap to reduce evaporation was used to perform the rheological measurements of as-prepared fresh pastes. Two different measurements were performed: i) flow curves (controlled rate measurements); here, ramp times of 6 s were recorded in the shear rate range between 2 and 100 s^{-1}, for a total of 12 ramps. A further decrease from 100 to 2 s^{-1} shear rate was performed by following the same ramp times. ii) viscosity vs. time measurements, at a fixed shear rate of 4 s^{-1}, for a maximum time of 150 min. Prior to any rheological measurement, all pastes were pre-sheared for 30 s at 100 s^{-1} [33] and held at 0 s^{-1} for 5 s in the viscometer.

2.2.2. Setting time

The setting time of every paste was determined using the Vicat test method according to UNE-EN 196-3:2005 (20ºC and 100% of relative humidity (RH)).

2.2.3. Impedance spectroscopy

A home-made cell capable to simultaneously measure temperature and impedance spectroscopy of cement pastes was used during the first 25 h of hydration [12]. It consists on an expanded polystyrene (EPS) hermetic prismatic shape-cell (30x30x50 mm^3) with two stainless steel electrodes placed inside. In all cases, 60 grams of cement paste were poured. Impedance spectra were obtained, at room temperature, using a frequency response analyzer (Solartron 1260) (frequency range of 5 Hz to 1 MHz) with an ac perturbation of 200 mV. Electrical data were taken every 15 min. The ZView program was used to analyze the spectra [34]. A K type-thermocouple (± 1ºC), placed in the middle of the cell, was used to measure the temperature.

2.2.4 Laboratory X-Ray Powder Diffraction (LXRPD).

On the one hand, *in-situ* LXRPD studies were performed on pastes during the first 16 hours of hydration in a MHC-trans multisample humidity chamber (25ºC and 95% RH) (Anton Paar), which works in transmission mode using molybdenum radiation. The amorphous (and free water) content was determined by adding ~20 wt% of quartz (ABCR, 99.56%), as an internal standard, previously to the anhydrous cement powder. Mo-Kα_1 powder patterns were collected on a D8 ADVANCE (Bruker AXS) diffractometer (188.5 mm of radius) prepared with a Johansson [Ge (111) primary monochromator], which provides a strictly monochromatic Mo radiation (λ=0.7093 Å) in transmission geometry (θ/θ) [35]. A constant volume was irradiated. The X-ray tube worked at 50 kV and 50 mA. The optics configuration was a fixed divergence slit (2 mm) and a fixed diffracted anti-scatter slit (9 mm). The energy-dispersive linear detector LYNXEYE XE 500 μm, optimized for high energy radiation, was used with the maximum opening angle. Using these conditions the samples were measured between 2-27º (2θ) with a step size of 0.01º and with a total measurement time of 15 min.

On the other hand, LXRPD studies were performed, at 1 and 7 days of hydration, on both anhydrous cement and cement pastes (after stopping hydration). Patterns were recorded on an X'Pert MPD PRO diffractometer (PANalytical) in reflection geometry ($\theta/2\theta$) using strictly

monochromatic CuKα_1 radiation (λ=1.54059Å) [Ge(111) primary monochromator]. The X-ray tube worked at 45 kV and 40 mA. The optics configuration was a fixed divergence slit (1/2°), a fixed incident antiscatter slit (1°), a fixed diffracted anti-scatter slit (1/2°) and X'Celerator RTMS (Real Time Multiple Strip) detector working in scanning mode with maximum active length. Data were collected, during ~2 hours, from 5º to 70° (2θ). The samples were rotated at 16 rpm to enhance particle statistics. G-factor approach [36,37] requires the collection of an external standard pattern in identical diffractometer configuration/conditions than the sample and as close in time as possible to the measurements to determine the diffractometer constant. A polished polycrystalline quartz rock was placed in the diffractometer in the very same orientation and a pattern was collected with the same experimental set up detailed above except for the spinning of the sample. The suitability of this quartz-rock was tested against NIST standard reference material SRM-676a (α-Al_2O_3) [38].

2.2.5. LXRPD Data Analysis.

LXRPD patterns of all samples were analyzed by the Rietveld method using the GSAS software package [39] to obtain the Rietveld quantitative phase analysis (RQPA). The refined overall parameters were: zero-shift error, peak shape parameters, cell parameters, phase scale factors and preferred orientation when appropriated. Peak shapes were fitted through the pseudo-Voigt function [40] corrected for axial divergence [41]. The Amorphous and Crystalline non-quantified (ACn) content of the stopped-hydration samples was determined through the external standard method (G-factor) for pastes at 1 and 7 days of hydration after stopping hydration (reflection mode) [36,37,42]. ACn content computes not only the amorphous fraction but also any non-computed crystalline phase and any misfit problem (for instance the lack of an adequate structural description for a given phase).

The internal standard method [42] has been used to determine not only ACn content but also the amount of free water in the *in-situ* study.

2.2.6. Thermal analysis.

Differential thermal (DTA) and thermogravimetric (TGA) analyses of ground fractions (~$40x10^{-3}$ g) of every paste at the hydration times of 1 and 7 days (after stopping hydration), were carried out in a SDT-Q600 analyzer (TA instruments, New Castle, DE). The temperature was increased from room temperature (RT) to 1000ºC at 10 ºC/min. The study was performed in an open platinum crucible under nitrogen flow. The weight lost from RT to 600ºC was considered as chemically bounded water and that from 600 to 1000ºC was assumed to be CO_2.

2.2.7. Compressive strengths.

Standard mortars with water/CSA/sand ratios of 0.5/1/3 were mechanically homogenized according to EN196-1. CEN standard sand (DIN EN 196-1) was used. Cubic samples of 30×30×30 mm^3 were cast and then de-aired in a jolting table (Model UTCM-0012, 3R, Montauban, France) with a total of 120 knocks. Molds were half cast and knocked for 60 times for a better homogenization. After that, they were fully cast and other 60 knocks were carried out. The cubes were kept at 20±1ºC and 99% RH during 24 hours. Subsequently, samples were demolded and left within a water bath at 20±1ºC until measurements were performed. Compressive strengths of mortars were measured at 1, 3, 7 and 28 days in a compression press (Model Autotest 200/10 W, Ibertest, Madrid, Spain) according to EN196-1 and at a rate of 1.5 $MPa \cdot s^{-1}$. The reported values are the average of three broken cubes. The as-obtained compressive strength values were corrected by a factor of 1.78; this factor is obtained by dividing the compression area of the machine (1600 mm^2) by the specimen area (900 mm^2).

2.2.8. Scanning Electron Microscopy (SEM).

The fracture cross-sections of the cement pastes with the optimized amount of each additive, at 1 day of hydration, were observed by scanning electron microscopy, SEM, (JEOL-JSM-840, Tokyo, Japan). Prior to SEM observation, the hydration of those samples was stopped by immersing them in isopropanol for 3 days and then heated at 40°C for 24 hours. The samples were gold sputtered.

2.2.9. Mercury Intrusion Porosimetry (MIP).

The porosity of the cement pastes with the optimized amount of each additive, at 1 and 7 days of hydration, after stopping hydration as described in 2.2.8 section, was measured through mercury porosimetry (MP) using a Quantachrome (Autoscan 33, Boynton Beach, Florida, US) porosimeter. The corresponding pastes without any additive were also measured for the sake of comparison. The assumed contact angle for data evaluation was 130°.

3. Results and Discussion

3.1 Rheological study.

Fig. 1 shows the deflocculation curves of CSA pastes with different amounts of the three additives: PC, TA and PA. All viscosity values were taken, at 50 s^{-1} , from the up-curves of the corresponding flow curves. The viscosity value of the paste without any additive is also shown for the sake of comparison. Pastes with similar viscosity values (0.9, 1.1 and 1.1 Pa·s at 50 s^{-1}) were prepared by adding 0.04, 0.15, and 0.15 wt% of PC, TA and PA, respectively. Thus, PC resulted as the most efficient additive in reducing viscosity at early ages in terms of active matter contents. In addition, the paste with 0.10 wt% of PC showed the minimum value of viscosity (0.1 Pa·s at 50 s^{-1}) within the studied experimental conditions. In the case of the other families, TA and PA-pastes, minimum values of viscosity were found when 0.15 and 0.20 wt% of the corresponding additives were added (1.1 and 0.8 Pa·s at 50 s^{-1}, respectively). However, the latter showed an important rheopectic cycle (625 Pa s^{-1}); this was reduced by 8 times, up to 79 Pa s^{-1}, by adding a total of 0.30 wt% of PA while keeping similar viscosity, and thus, improving the stability of the paste.

Figs. 2.a, 2.b and 2.c show the evolution of viscosity with time of pastes with different amounts of PC, TA and PA, respectively, at 4 s^{-1}. The selected shear rate is low enough for not destroying the structure and high enough for obtaining trustable data. The viscosity of all these pastes increased with time, as expected. The behavior with time of the paste without additive was not possible to be measured due to the combination of its high viscosity and fast setting time. On the one hand, PC-pastes (Fig. 2.a) do not show a significant delay in viscosity increase when small amounts of superplasticizer were added, e.g. 0.04 and 0.05 wt%, although the initial viscosity slightly decreased

by increasing the addition of additive (Fig. 1). However, by increasing this additive content, from 0.10 to 0.35 wt% of PC, the rising in viscosity is harshly delayed. On the other hand, the rising in viscosity with time of pastes with 0.15, 0.20 or even 0.45 wt% of TA (Fig. 2.b) was not affected by those studied TA contents. In addition, the evolution with time of these pastes resulted to be between pastes with 0.05 and 0.10 wt% of PC.

In the case of pastes with PA (Fig. 2.c), the viscosity also increases with time, as expected, and that rising in viscosity is delayed by increasing the additive content. PA-pastes show a local minimum of viscosity after 17 or 33 minutes when 0.15 or 0.30 wt% of PA, respectively, were added. That local minimum may represent a stable zone where the structure of aggregates is being destroyed by shear stress, and viscosity rises again when hydration progresses and the bonding strength between particles increases [43].

This rheological characterization allows the design of pastes (type and amount of additive), and thus mortars, with different evolution of viscosity (and setting time) maintaining a good flowability.

When pastes with the same amount of active matter of additive, e.g. 0.15 wt%, are compared, PC is the most effective retarder, followed by PA-paste, and finally, TA-paste. Within the first 16 minutes, the viscosity of both TA and PA pastes rise in a similar way, but after that, their viscosities develop differently. These different trends may well be related to the number of anchor sites, where the highest one is for polycarboxylate, followed by the phosphonic acid (a maximum of 6 sites at alkaline pH values) [44], and tartaric acid (a maximum of 4 sites at alkaline pH) [45].

Pastes with 0.10, 0.15 and 0.30 wt% of PC, TA and PA, respectively, were selected and further compared since they show the minimum initial viscosity value and rheopectic cycle of each family with an adequate delay in rising viscosity with time. For a better/easier comparison, Fig. 2.d depicts the evolution of viscosity with time of those selected pastes. The paste with 0.10 wt% PC presented the lowest viscosity during the first 30 minutes of hydration; after that time it showed a sharp increase until 400 Pa·s. However, the paste with 0.30 wt% of PA showed the slowest rising of

viscosity after the first 30 min, and it takes around 100 minutes to gain 400 Pa·s. Finally the viscosity of the paste with 0.15 wt% TA increased quickly, 20 min, from the beginning.

3.2 Setting time and impedance spectroscopy results.

Table 1 reports the initial and final setting times of the three selected pastes from the VICAT measurements. The corresponding values for the paste without any additive are also shown for the sake of comparison. The setting time shows the same trend explained before for the viscosity curves, where the addition of PA delays considerably the initial setting time, and PC and TA pastes show similar setting values.

A deeper study was performed on these selected pastes (0.10, 0.15 and 0.30 wt% of PC, TA and PA, respectively) by impedance spectroscopy. As an example, Fig. 3.a shows the complex impedance plots as a function of time for the TA-paste. Similar plots were obtained for the other selected pastes and the only difference consists on the absolute value of resistance. At short hydration times, pastes show high conductivity values and low frequency effects were observed in the form of an inclined spike. Conductivity decreases with the hydration time, thus data show a single broad arc at high frequencies, which size increases with time. The total resistance data are obtained from the interception of the spike and/or the arc (low frequency end) on the Z' axis. In all cases, the resistance increases approximately 4 orders of magnitude after 25 hours due to the gradual hydration of the pastes. Initial conductivity values of 2.8×10^{-3}, 2.6×10^{-3} and 3.3×10^{-3} $S \cdot cm^{-1}$, and final conductivity data of 2.2×10^{-5}, 8.1×10^{-6} and 2.1×10^{-4} $S \cdot cm^{-1}$ were obtained for PC, TA and PA pastes, respectively. PC and TA pastes show similar initial conductivity values; PA-paste shows the highest value of initial conductivity, which is related to the highest concentration of ions in dissolution. These data were taken at 10 min of hydration, time required for tunning the conductivity system. At the end of the measurement (after 25 h), the obtain final conductivity is almost negligible, being slightly higher for the PA-mortar, in agreement with the longest setting time, and hence higher amounts of ions in water pores.

Conductivity data were also converted to a normalized form called conversion fraction (α), ranging from 0 to 1, to study the progress of the reaction with time. The conversion fraction at different hydration times $\alpha(t)$ was calculated using the relative change in the electrical conductivity during hydration using the following empirical equation:

$$\alpha(t)= \sigma_0-\sigma\ (t)/(\sigma_0-\sigma_\infty) \quad \text{Eq. (4)}$$

where σ_0 and σ_∞ are the respective conductivities at the beginning and the end of the transformation process, respectively, and $\sigma(t)$ is the conductivity at time t between these two limits. Fig. 3.b shows the evolution of the conversion fraction with time for the three selected pastes within the first 25 hours of hydration. These profiles were mathematically fitted by a non-linear regression model using the following Boltzmann sigmoidal model, shown in Eq. (5):

$$\alpha(t) = \alpha_0 + \frac{\alpha_\infty - \alpha_0}{1+e^{\frac{t-t_0}{\Delta t}}} \quad \text{Eq. (5)}$$

Where α_0 and α_∞ are the conversion fraction at the beginning and after network formation at long times, respectively. The induction time, t_0, corresponds to the time necessary to reach a conversion fraction of 0.5 and Δt, the time or rate which describes the steepness of the curve, with a large value denoting a shallow curve. The latter corresponds to the "rate of conversion" related to the electrical conductivity of the material. These parameters are marked in Fig. 3.b for PA-paste.

Many authors have used a Boltzmann sigmoidal model to describe viscous fluids undergoing a setting reaction including starch, photopolymerizable acrylates and gels [46,47,48]. In our case, the Boltzmann sigmoidal model represents successfully the dynamics of the hydration of the three pastes with R^2 correlation factors higher than 0.999. PA-paste presents both the largest induction (414 min) and "rate of conversion" (135 min) times. When 0.10 wt% of PC was added to the paste, lower values of induction (170 min) and "rate of conversion" (19 min) times were found. Finally, the TA-paste shows the fastest reaction kinetics with the lowest values of both induction (101 min) and "conversion" (14 min) times. These results are in full agreement with the viscosity curves (Fig.

2.d). Fig. 3.c shows the variation of temperature (related to the heat released during hydration) in the measuring cell. The temperature of all pastes increases up to a maximum value, which corresponds to a transformation of α~0.5. This rising in temperature happens firstly to the TA-paste (145 min), secondly to the PC-paste (215 min), and finally for the PA-paste, in agreement with Figs. 2.d and 3.b. To understand this behavior in-situ LXRPD of the pastes during the first hours of hydration has been performed.

3.3 Phase assemblage (laboratory x-Ray powder diffraction).

It is known that the transformation of bassanite into gypsum will increase both the viscosity and temperature of pastes at early ages of hydration. The control of this transformation may be a key issue for tailoring the hydration of the pastes. Figs. 4.a and 4.b show the evolution of bassanite and gypsum with time, respectively, obtained from RQPA of the in-situ LXRPD study, of all the selected pastes, including the paste without additives. The transformation (dissolution of bassanite/precipitation of gypsum) happens quickly in the paste without additives, with the consequent dramatic effects (higher viscosity and inhomogeneity of samples). However, the formation of gypsum is delayed with the presence of additives; the transformation happens firstly in TA-paste, secondly in PC-paste, and finally in PA-paste, justifying the tendency in increasing both viscosity with time (Fig. 2.d) and temperature (Fig. 3.c). In addition, the lowest amount of gypsum formed in PA-paste is in agreement with the lowest temperature achieved (Fig. 3.c).

Table 2 reports RQPA results for the three selected pastes at 1 and 7 days of hydration. The table includes both ACn and free water (FW) contents. The weighed loss data obtained from DTA–TGA measurements from RT to 600ºC are also included. Fig. 5 shows the Rietveld plot of the PC-paste at 7 days of hydration where the major peaks of each phase are labeled, as a representative example. The Rietveld plots of the remaining pastes at 1 and 7 days of hydration as provided as Supplementary Information (Figures S1-S4). From Table 2, it can be seen that bassanite has disappeared and has been transformed into gypsum before 1 day of hydration. After 1 day of hydration, similar amounts of AFt were formed in the three systems (between 21 and 25 wt%) and,

after 7 days, the formed amounts were also similar (between 35 and 40 wt%) in all pastes. Thus, phase assemblage at later ages was not dramatically affected by the type of retarder at these hydration ages.

3.4 Compressive strength development, porosimetry and SEM.

The mechanical behavior of the corresponding mortars was also studied. Fig. 6 gives the compressive strength values of mortars prepared with the optimum amount of each retarder (0.10, 0.15 and 0.30 wt% of PC, TA and PA, respectively), and without any additive, for the sake of comparison. The low values of the latter are due to the heterogeneity of the samples related to their short setting time (and high viscosity) related to the fast transformation of bassanite into gypsum. The addition of selected amounts of retarders has resulted in homogeneous mortars with high mechanical strengths: between 38 and 46 MPa at 1 day of hydration, and between 75 and 85 MPa at 7 days of hydration. At 1 day of hydration, TA and PA mortars show slightly higher strength values than PC although the three corresponding pastes show similar open porosity values (~34 vol%) and similar median pore diameter (volume) (~110 nm); then that behavior may be related to their longer final setting time (Table 1) which provides with higher plasticity to the TA-system, allowing the better accommodation of ettringite [12]. PA-mortars show compressive strength values similar to TA-mortars since the better accommodation of ettringite is compensated with the very long final setting time (300 min). This was confirmed through SEM observations. As an example, Fig. S5 (deposited as Supplementary Information) shows the SEM micrographs of fracture surfaces of PC (a) and PA (b) pastes at 1 day of hydration after stopping hydration; the particle size of ettringite in the former is considerably smaller than in the latter, although both mortars contain the same amount of ettringite (Table 2). Shi et al. also observed ettringite particles with different size and morphology by adding different additives [29].

At 7 days of hydration, PA-mortar has the lowest compressive strengths; although the three pastes showed similar open porosity values (~30 vol%), PA-pastes show the highest values of median pore

diameter (volume) (being 150, 100 and 273 nm for PC, TA and PA-pastes, respectively), which reduce the mechanical properties of the corresponding mortars.

These results point out PC as the best additive used in CSA mortars with bassanite for engineering applications when high compressive strength values are needed at hydration times larger than 3 days. However, if high strength values are demanded at earlier curing ages, any of them can be used. The compressive strength values of mortars prepared with the combination of bassanite and retarders are even better than those prepared with gypsum or anhydrite without additives at any hydration time. For instance, bassanite mortars (with PC or TA) show compressive values of 84 MPa at 7 days of hydration, higher than the corresponding values for mortars prepared with gypsum or anhydrite (65 and 70 MPa, respectively [12]).

4. Conclusions

Bassanite-CSA pastes show high water demand, high viscosity values and short setting times which has a dramatic effect onto the mechanical strength values of the corresponding mortars. It makes necessary the selection of a hydration retarder which also reduces the viscosity of the pastes.

The effect of three additives (polycarboxylate, tartaric acid and phosphonic acid) on CSA pastes and mortars has been studied. The amount of each additive was firstly optimized (0.10, 0.15 and 0.30 wt% of polycarboxylate (PC), tartaric acid (TA) and phosphonic acid (PA), respectively). All of them improved the workability of pastes, where the polycarboxylate is the best additive in reducing viscosity at very early ages (within the first 30 min of hydration). For the selected amounts, phosphonic acid resulted as the additive that most delay setting times, and pastes with polycarboxylate and tartaric acid show similar setting values.

The use of different additives also affected the dissolution of ions and achieved temperature; thus, the phosphonic acid-paste shows the highest value of initial conductivity and suffers from a lower increasing in temperature that happens at longer hydration times. All these factors are related to the transformation of bassanite into gypsum which happens at later ages, and longer setting times.

The control of all these parameters allows the improvement of the mechanical strengths. For instance, mortars with 0.10 wt% polycarboxylate show the highest values of compressive strength at hydration times ≥ 3 days (71 and 84 MPa at 3 and 7 days, respectively); however, at earlier ages (1 day), the three mortars show similar compressive values, slightly lower for the polycarboxylate ones (38, 46 and 44 MPa, for polycarboxylate, tartaric acid and phosphonic acid pastes, respectively).

All these parameters can be controlled, making possible the design and preparation of mortars with selected properties for specific engineering applications.

Acknowledgments

Funding from Junta de Andalucía (P11-FQM-7517 and P12-FQM-1656), FEDER/University of Málaga (FC14-MAT-23), MINECO (BIA2014-57658-C2-1-R and BIA2014-57658-C2-2-R, the latter co-funded by FEDER) are acknowledged.

REFERENCES

[1] E. Gartner, Industrially interesting approaches to "low-CO_2" cements, Cem. Concr. Res. 34(9) (2004) 1489-1498.

[2] J.H. Sharp, C.D. Lawrence, R. Yang, Calcium sulphoaluminate cements – Low-energy cements, special cements or what?. Adv. Cem. Res. 11 (1999) 3-13.

[3] C.D. Popescu, M. Muntean, J.H. Sharp, Industrial trial production of low energy belite cement, Cem. Concr. Comp. 25(7) (2003) 689-693.

[4] E. Worrell, L. Price, N. Martin, C. Hendriks, L.O. Meida, Carbon dioxide emissions from the global cement industry. Ann. Rev. Energy Environ. 26 (2001) 303–329.

[5][5] M.A.G. Aranda, A.G. De la Torre, Sulfoaluminate cement, in: Pacheco-Torgal F, Jalali S, Labrincha J, John VM (Eds). Eco-efficient Concrete, Woodhead Publishing Limited. Cambridge, 2013, pp. 488-522.

[6] I. Odler, Special Inorganic Cements, London: Taylor & Francis, 2000.

[7] S. Sahu, J. Majling, Phase compatibility in the system $CaO–SiO_2–Al_2O_3–Fe_2O_3–SO_3$ referred to sulphoaluminate belite cement clinker. Cem. Concr. Res. 23(6) (1993) 1331-1339.

[8] J. Pera, J. Ambroise, New applications of calcium sulfoaluminate cement, Cem. Concr. Res. 34(4) (2004) 671-676.

[9] F. Winnefeld, S. Barlag, Calorimetric and thermogravimetric study on the influence of calcium sulfate on the hydration of ye´elimite. J. Therm. Anal. Calorim. 101(3) (2009) 949-957.

[10] S. Sahu, J. Havlica, V. Tomková, J. Majling, Hydration behaviour of sulphoaluminate belite cement in the presence of various calcium sulphates. Thermochim Acta 175(1) (1991) 45-52.

[11] M. Marchi, U. Costa, Influence of the calcium sulphate and w/c ratio on the hydration of calcium sulphoaluminate cement, Proceedings of the 13th international Congress Chem. Cem. Madrid (Spain), 2011.

[12] M. García-Maté, A.G. De la Torre, L. Leon-Reina, E.R. Losilla, M.A.G. Aranda, I. Santacruz, Effect of calcium sulfate source on the hydration of calcium sulfoaluminate eco-cement, Cem. Concr. Comp. 55 (2015) 53-61.

[13] S. Allevi, M. Marchi, F. Scotti, S. Bertini, C. Cosentino, Hydration of calcium sulphoaluminate clinker with additions of different calcium sulphate sources, Mater. Struct. 49(1) (2016) 453-466.

[14] F. Puertas, H. Santos, M. Palacios, S. Martínez-Ramírez, Polycarboxylate superplasticiser admixtures: effect on hydration, microstructure and rheological behaviour in cement pastes, Adv. Cem. Res. 17(2) (2005) 77-89.

[15] J. Cheung, A. Jeknavorian, L. Roberts, D. Silva, Impact of admixtures on the hydration kinetics of Portland cement, Cem. Concr. Res. 41(12) (2011) 1289-1309.

[16] W. Hanley, D. Constantiner, J. Goldbrunner, Retarder for calcium sulphoaluminate cements, US Patent 6,818,057 B2, 16 November 2004.

[17] M. Bishop, A.R. Barron, Cement hydration inhibition with sucrose, tartaric acid and lignosulfonate: analytical and spectroscopic study, Ind. Eng. Chem. Res. 45(21) (2006) 7042-7049.

[18] N.L. Thomas, J.D. Birchall, The retarding action of sugars on cement hydration, Cem. Concr. Res. 13(6) (1983) 830-842.

[19] P. Juilland, E. Gallucci, R. Flatt, K. Scrivener, Dissolution theory applied to the induction period in alite hydration, Cem. Concr. Res. 40 (2010) 831–844.

[20] M. Bishop, S.G. Bott, A.R. Barron, A new mechanism for cement hydration inhibition: solid-state chemistry of calcium nitrilotris(methylene)triphosphonate, Chem. Mater. 15 (2003) 3074–3088.

[21] W. Chang, H. Li, M. Wei, Z. Zhu, J. Zhang, M. Pei, Effects of polycarboxylic acid based superplasticiser on properties of sulphoaluminate cement, Mater. Res. Innovations 13(1) (2009) 7-10.

[22] J. Gołaszewski, Influence of cement properties on new generation superplasticizers performance, Constr. Build. Mater. 35 (2012) 586-596.

[23] F. Ridi, L. Dei, E. Fratini, S.H. Chen, P. Baglioni, Hydration kinetics of tri-calcium silicate in the presence of superplasticizers, J. Phys. Chem. 107(4) (2003) 1056-1061.

[24] J. Rieger, J. Thieme, C. Schmidt, Study of precipitation reactions by X-ray microscopy: $CaCO_3$ precipitation and the effect of polycarboxylates, Langmuir 16 (2000) 8300-8305.

[25] S. Hanehara, K. Yamada, Rheology and early age properties of cement systems, Cem. Concr. Res. 38(2) (2008) 175-195.

[26] K. Yamada, S. Ogawa, S. Hanehara, Controlling of the adsorption and dispersing force of polycarboxylate-type superplasticizer by sulfate ion concentration in aqueous phase, Cem. Concr. Res. 31(3) (2001) 375-383.

[27] J. Plank, Z. Dai, P.R. Andres, Preparation and characterization of new Ca–Al–polycarboxylate layered double hydroxides, Mater. Lett. 60(29-30) (2006) 3614-3617.

[28] C. Giraudeau, J.B.E. Lacaillerie, Z. Souguir, A. Nonat, R. Flatt, Surface and intercalation chemistry of polycarboxylate copolymers in cementitious systems, J. Am. Ceram. Soc. 92(11) (2009) 2471-2488.

[29] C. Shi, G. Zhang, T. He, Y. Li, Effects of superplasticizers on the stability and morphology of ettringite, Constr. Build. Mater.112 (2016) 261–266.

[30] M. García-Maté, I. Santacruz, A.G. De la Torre, L. León-Reina, M.A.G. Aranda, Rheological and hydration characterization of calcium sulfoaluminate cement pastes, Cem. Concr. Comp. 34 (2012) 684-691.

[31] M. García-Maté, A.G. De la Torre, L. León-Reina, M.A.G. Aranda, I. Santacruz, Hydration studies of calcium sulfoaluminate cements blended with fly ash, Cem. Concr. Res.54 (2013) 12-20.

[32] J. Wang, Hydration mechanism of cements based on low-CO_2 clinkers containing belite, ye´elimite and calcium alumino-ferrite. PhD Thesis. Lille, University of Lille, 2010.

[33]O.H. Wallevik, D. Feys, J.E. Wallevik, K.H. Khayat, Avoiding inaccurate interpretations of rheological measurements for cement-based materials, Cem. Concr. Res. 78 (2015) 100-109.

[34] D. Johnson, ZView: a software program for IES analysis, version 2.8, Scribner Associates Inc, Southern Pines, NC, 2008.

[35] L. León-Reina, M. García-Maté, G. Álvarez-Pinazo, I. Santacruz, O. Vallcorba, A.G. De la Torre, M.A.G. Aranda Accuracy in Rietveld quantitative phase analysis: a comparative study of strictly monochromatic Mo and Cu radiations, (2016) J. Appl. Cryst. 49, doi:10.1107/S1600576716003873.

[36] G. Álvarez-Pinazo, A. Cuesta, M. García-Maté, I. Santacruz, E.R. Losilla, A.G. De la Torre, L. León-Reina, M.A.G. Aranda, Rietveld quantitative phase analysis of yeelimite-containing cements, Cem. Concr. Res. 42(7) (2012) 960-71.

[37] D. Jansen, F. Goetz-Neunhoeffer, C.H. Stabler, J. Neubauer, A remastered external standard method applied to the quantification of early OPC hydration, Cem. Concr. Res. 41(6) (2011) 602-608.

[38] J.P. Cline, R.B. Von Dree, R. Winburn, P.W. Stephens, J.J. Filliben, Addressing the amorphous content issue in quantitative phase analysis: the certification of NIST standard reference material 676a, Acta Cryst. 67(4) (2011) 357-367.

[39] A.C. Larson, R.B. Von Dreele, General structure analysis system (GSAS). Los Alamos national laboratory report LAUR, 2004. p. 86-748.

[40] Thompson P, Cox DE, Hasting JB. Rietveld refinement of Debye–Scherrer synchrotron X-ray data from Al_2O_3. J Appl Crystallogr 1987;20:79-83.

[41] L.W. Finger, D.E. Cox, A.P. Jephcoat, A correction for powder diffraction peak asymmetry due to diaxial divergence, J. Appl. Crystallogr. 27 (1994) 892-900.

[42] M.A.G. Aranda, A.G. De la Torre, L. León-Reina, Powder diffraction characterisation of cements, in: International Tables for Crystallography, Gilmore C, Kaduk J, Schenk H, editors. Volume H-Powder Diffr, 2016, in press.

[43] T. Emoto, T.A. Bier, Rheological behavior as influenced by plasticizers and hydration kinetics. Cem. Concr. Res. 37(5) (2007) 647-654.

[44] K.D. Demadis, Phosphonates in Matrices, in: E. Brunet, J.L. Colón, A. Clearfield (Eds.), Tailored Organic-Inorganic Materials, John Wiley & Sons, Inc., Hoboken, New Jersey, 2015, pp. 83-134.

[45] T. Gelbrich, T.L. Threlfall, M.B. Hursthouse, Interplay between hydrogen bonding and metal coordination in alkali metal tartrates and hydrogen tartrates, CrystEngComm. 16 (2014) 6159-6169.

[46] K. Israkarn, P. Hongsprabhas, Influences of granule-associated proteins on physicochemical properties of mungbean and cassava starches, Carbohydr. Polym. 68 (2007) 314-322.

[47] B.J. Love, R.F. Piguet, F. Teyssandier, Chemorheology of photopolymerizable acrylates using a modified Boltzmann sigmoidal model, J. Polym. Sci. Pol. Phys. 46 (2008) 2319-2325.

[48] A.L. Navarro-Verdugo, F.M. Goycoolea, G. Romero-Meléndez, I. Higuera-Ciapara, W.A. Argüelles-Monal, A modified Boltzmann sigmoidal model for the phase transition of smart gels, Soft Matter. 7 (2011) 5847-5853.

Figure Captions

Fig. 1. Deflocculation curve of CSA pastes with the three additives, polycarboxylate (PC), phosphonic acid (PA) and tartaric acid (TA).

Fig. 2. Evolution of the viscosity with time of the pastes with different amounts of polycarboxylate (a), tartaric acid (b), phosphonic acid (c), and the comparative of pastes with 0.10, 0.15 or 0.30 wt% of PC, TA and PA (d).

Fig. 3. Complex impedance plots as a function of time for paste with 0.15 wt% of TA (a), evolution of the conversion fraction (b) and temperature (c) with time for the three selected pastes (0.10, 0.15 or 0.30 wt% of PC, TA and PA, respectively) within the first 25 hours of hydration of the same pastes. The solid line in Fig. 3b is the fitting result to the Boltzman sigmoidal model.

Fig. 4. Phase evolution of Bassanite (a), and Gypsum (b) (in weight percentage) with time, within the first 1000 min of hydration.

Fig. 5. Rietveld LXRPD plot (λ=1.54 Å) for the paste prepared with 0.10 wt% PC at 7 days of hydration.

Fig. 6. Compressive strength values of mortars prepared at different hydration times using retarders and superplastizicer (0.10, 0.15 or 0.30 wt% of PC, TA and PA, respectively). Results for the mortars without additives are also shown for the sake of comparison.

Table 1. Initial and final setting time of the selected pastes from Vicat test.

Paste	Initial setting time (min)	Final setting time (min)
w/o additives	20	60
0.10 wt% PC	65	85
0.15 wt% TA	65	120
0.30 wt% PA	180	300

Table 2. Rietveld quantitative phase analysis results in weight percentage (including ACn and FW) for the selected pastes as a function of hydration time. The data for paste without additives are also shown. Weighed loss values obtained from DTA–TGA measurements from RT to 600ºC are also included.

		w/o additive		0.10 wt% PC		0.15 wt% TA		0.30 wt% PA	
	0 d	1d	7d	1d	7d	1d	7d	1d	7d
$C_4A_3\underline{S}$	25.5(1)	11.4(1)	4.8(1)	9.5(1)	3.7(1)	9.8(1)	4.3(1)	12.8(1)	4.3(1)
$C\underline{S}H_{0.5}$	12.1(2)	-	-	-	-	-	-	-	-
$C\underline{S}H_2$	-	8.5(1)	4.2(1)	7.5(1)	3.9(1)	7.9(1)	4.4(1)	10.0(1)	4.7(1)
β-C_2S	8.6(3)	10.9(2)	11.4(2)	10.8(2)	11.9(2)	11.7(3)	11.4(3)	11.4(3)	12.4(3)
Arkemanite	0.3(1)	0.4(1)	0.3(1)	0.2(1)	0.3(1)	0.3(1)	0.3(1)	0.4(1)	0.3(1)
Minor phases[$]	4.9(1)	2.4(1)	2.1(1)	2.0(1)	2.2(1)	2.6(1)	2.1(1)	2.7(1)	2.5(1)
AFt	-	20.6(1)	34.7(1)	21.8(1)	38.4(1)	25.4(1)	37.9(1)	21.2(1)	40.5(1)
AH_3	-	0.5(1)	0.7 (1)	0.5(1)	1.0(1)	0.7(1)	0.9(1)	0.7(1)	1.0(1)
Vaterite	-	0.3(2)	0.4(2)	0.5(2)	0.6(2)	1.0(2)	0.6(2)	0.9(2)	0.7(2)
ACn	15.3(3)	34.6(4)	38.3(4)	38.1(4)	36.3(4)	31.7(4)	35.7(4)	29.0(4)	31.3(4)
FW	33.3	10.3	3.0	9.0	1.6	8.9	2.3	10.9	2.3
SUM	100.0	100.0	100.0	100.0	100.0	100.0	100.0	100.0	100.0
Weighed loss-600°C / % (stopped hydration)	-	24.0	31.3	25.3	32.7	25.4	32.0	23.4	32.0

[$]Overall amount of cement crystalline minor phases: C_4AF, $C\underline{S}$, $CaTiO_3$ and MgO.

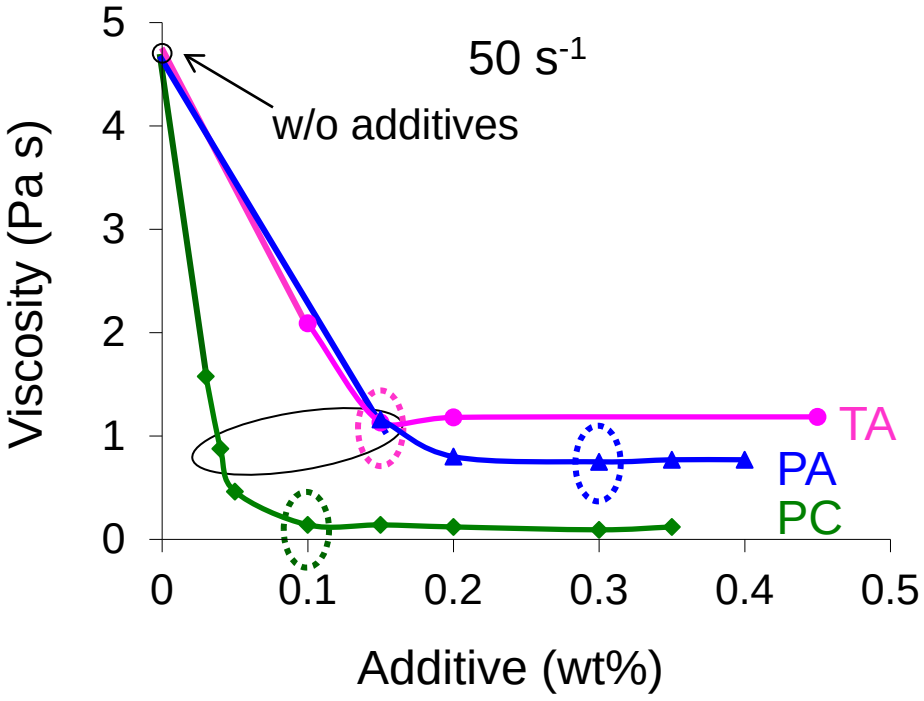
50 s-1
w/o additives
Viscosity (Pa s)
5
4
3
2
1
0
0
0.1
0.2
0.3
0.4
0.5
Additive (wt%)
TA
PA
PC

Fig. 1

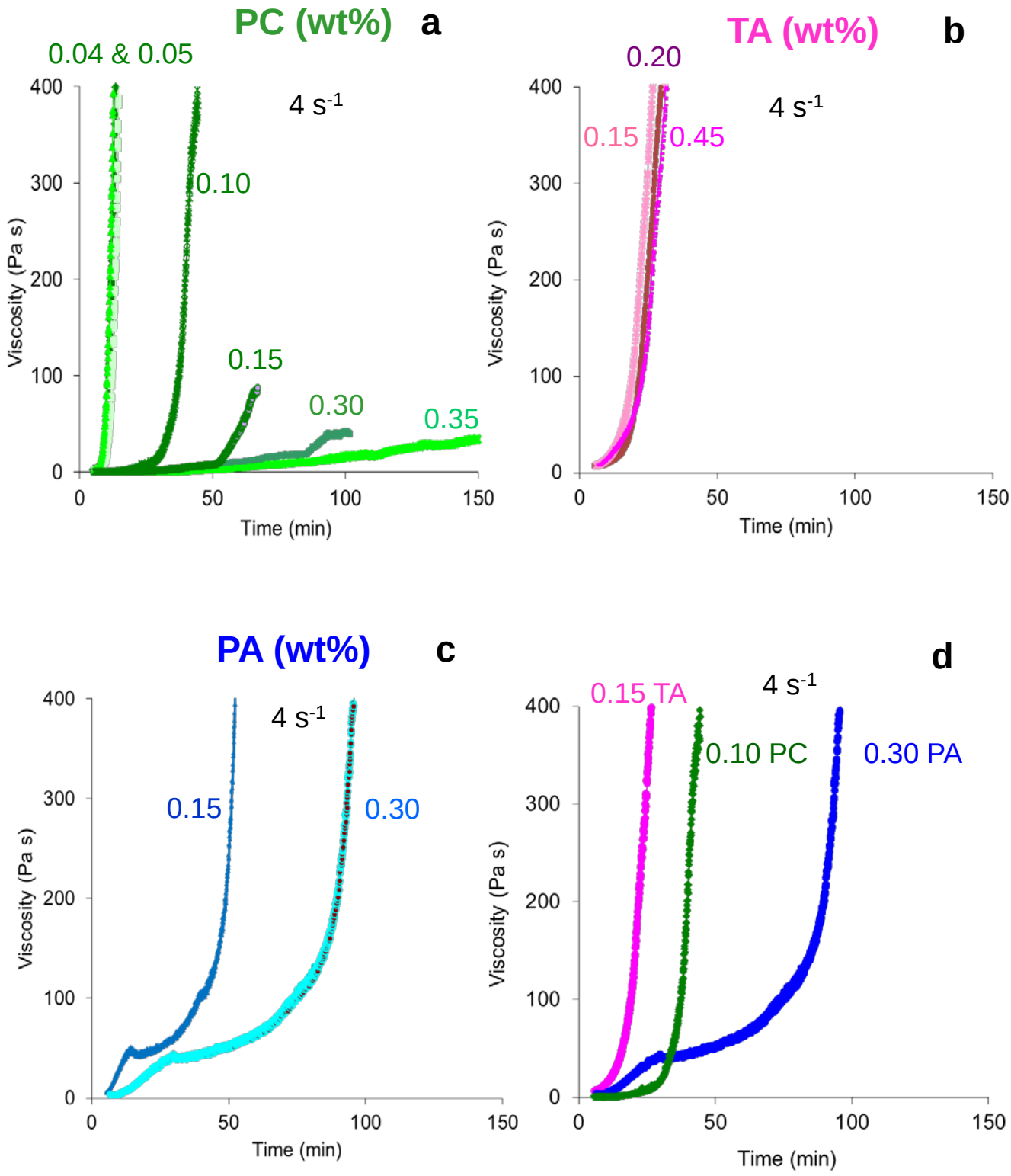
PC (wt%)
a
0.04 & 0.05
4 s-1
0.10
0.15
0.30
0.35
Viscosity (Pa s)
Time (min)
TA (wt%)
b
0.20
0.15
0.45
4 s-1
Viscosity (Pa s)
Time (min)
PA (wt%)
c
4 s-1
0.15
0.30
Viscosity (Pa s)
Time (min)
d
0.15 TA
4 s-1
0.10 PC
0.30 PA
Viscosity (Pa s)
Time (min)

Fig. 2

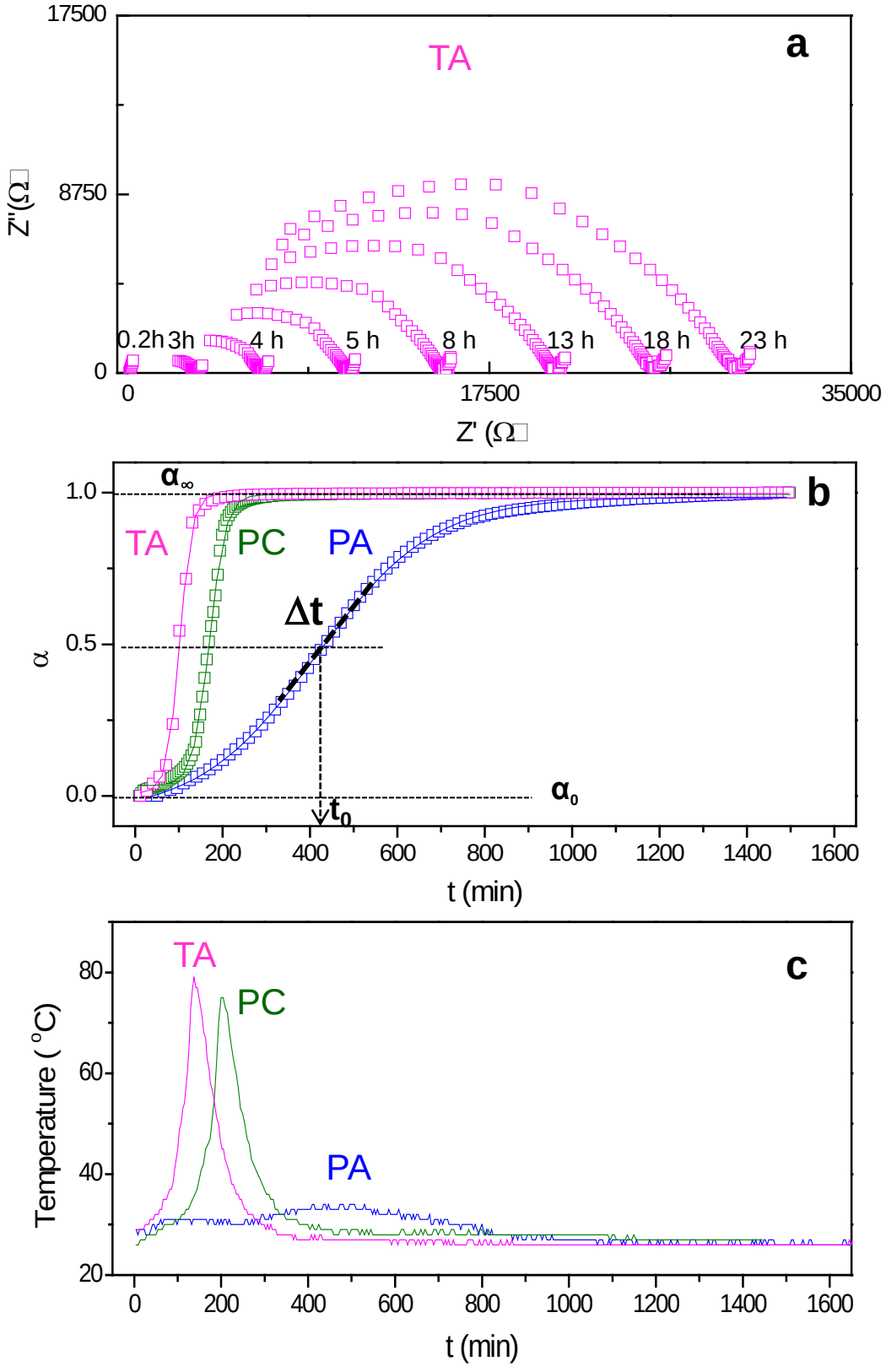
a
TA
17500
8750
0
Z''(Ω)
0.2h
3h
4 h
5 h
8 h
13 h
18 h
23 h
0
17500
35000
Z' (Ω)
b
α∞
1.0
0.5
0.0
α
TA
PC
PA
Δt
t0
α0
0
200
400
600
800
1000
1200
1400
1600
t (min)
c
TA
PC
PA
80
60
40
20
Temperature (°C)
0
200
400
600
800
1000
1200
1400
1600
t (min)

Fig. 3

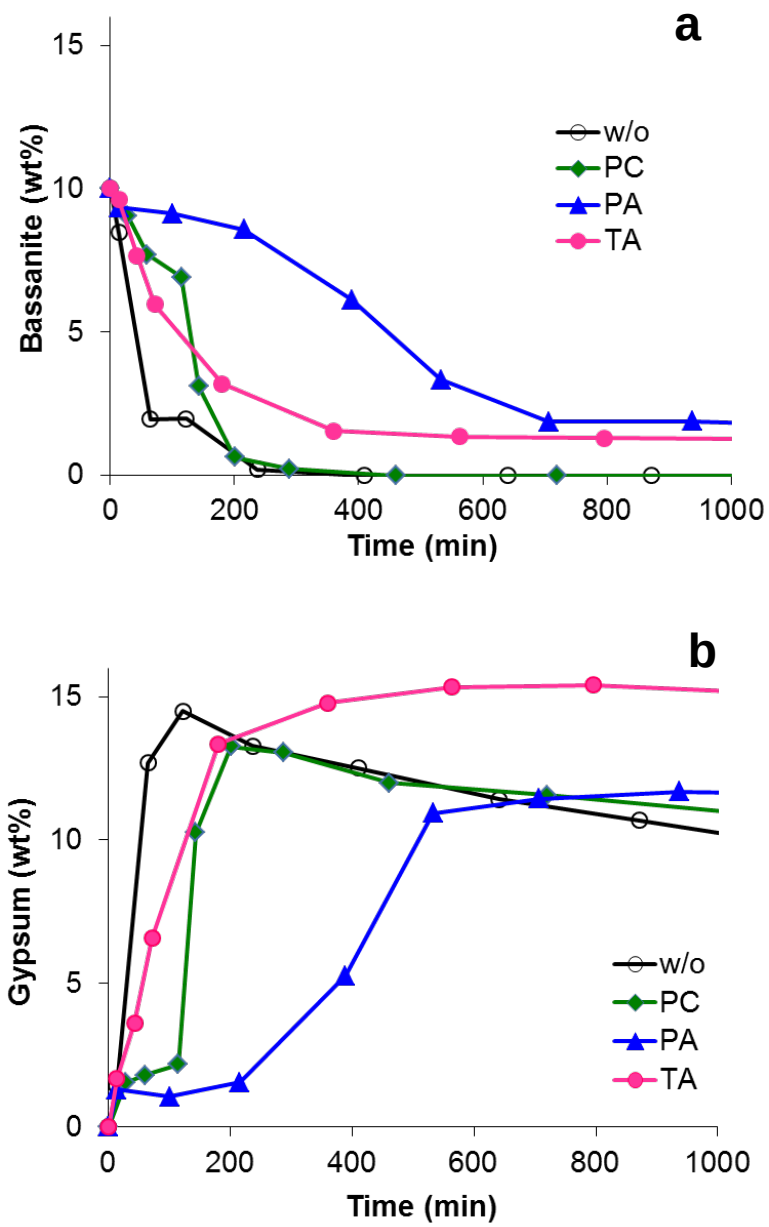
a
Bassanite (wt%)
15
10
5
0
0
200
400
600
800
1000
Time (min)
w/o
PC
PA
TA
b
Gypsum (wt%)
15
10
5
0
0
200
400
600
800
1000
Time (min)
w/o
PC
PA
TA

Fig. 4

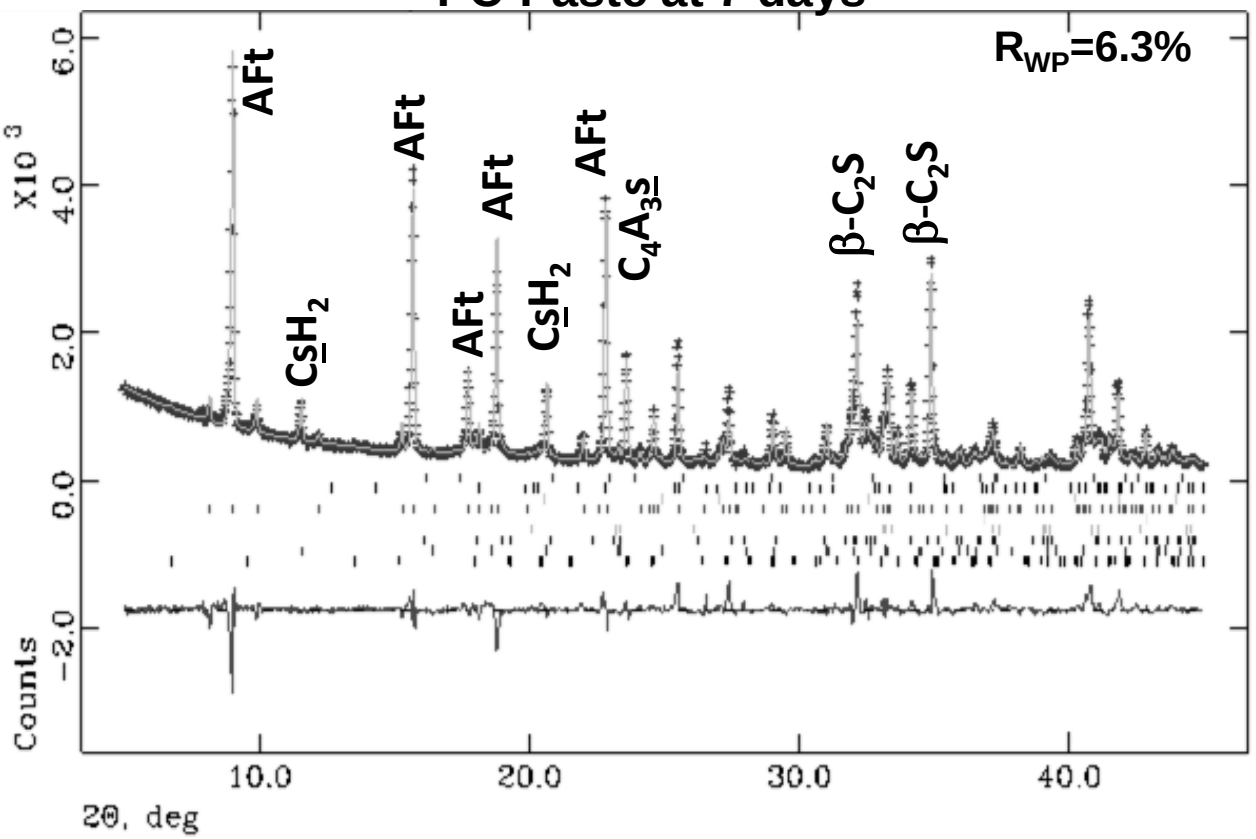
PC-Paste at 7 days
R_{WP}=6.3%
AFt
AFt
AFt
AFt
$C\underline{S}H_2$
$C\underline{S}H_2$
$C_4A_3\underline{S}$
β-C_2S
β-C_2S
X10 3
6.0
4.0
2.0
0.0
−2.0
Counts
10.0
20.0
30.0
40.0
2θ, deg

Fig. 5

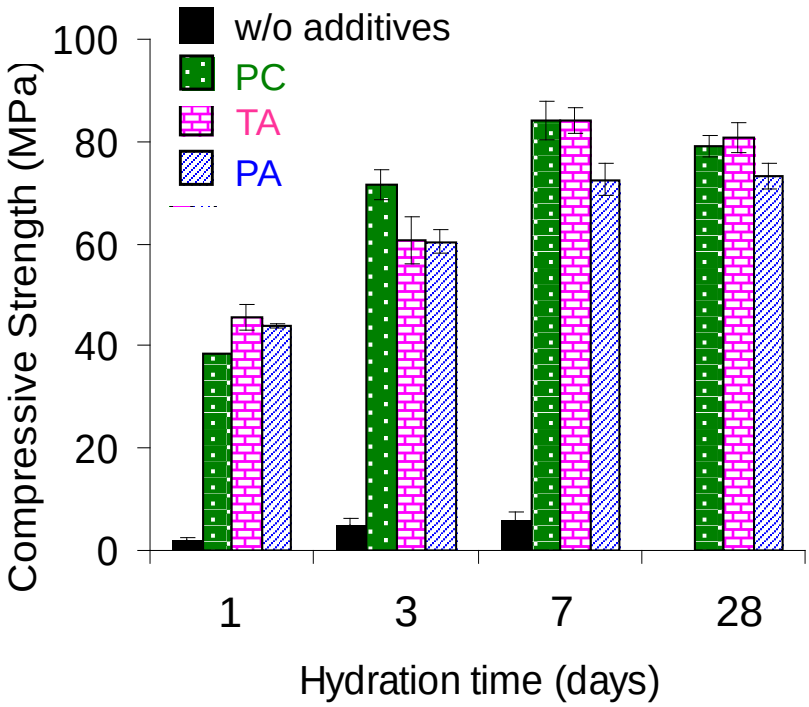
w/o additives
PC
TA
PA
Compressive Strength (MPa)
100
80
60
40
20
0
1
3
7
28
Hydration time (days)

Fig. 6

Supplementary Information

Tailored setting times with high compressive strengths in bassanite calcium sulfoaluminate eco-cements

M. García-Maté[1], D. Londono-Zuluaga[1], A. G. De la Torre[1], E.R. Losilla[1], A. Cabeza[1], M. A. G. Aranda[1,2] and I. Santacruz[*,1]

[1] Departamento de Química Inorgánica, Cristalografía y Mineralogía, Universidad de Málaga, 29071-Málaga, Spain

[2] CELLS-Alba synchrotron, Carretera BP 1413, Km. 3.3, E-08290 Cerdanyola, Barcelona, Spain

Fig. S1. Rietveld LXRPD plot (λ=1.54 Å) for the anhydrous cement.

Fig. S2. Rietveld LXRPD plot (λ=1.54 Å) for the paste prepared with 0.10 wt% of polycarboxylate at 1 day.

Fig. S3. Rietveld LXRPD plot (λ=1.54 Å) for the paste prepared with 0.15 wt% of tartaric acid at 1 day (a), and 7 days (b) of hydration.

Fig. S4. Rietveld LXRPD plot (λ=1.54 Å) for the paste prepared with 0.30 wt% of phosphonic acid at 1 day (a), and 7 days (b) of hydration.

Fig. S5. SEM micrographs of fracture surfaces of PC (a) and PA (b) pastes at 1 day of hydration.

Table S1. X-ray fluorescence analysis for both raw materials (CSA clinker and gypsum).

[*] Corresponding author. Tel.: +34952131992; fax: +34952131870. *E-mail:* isantacruz@uma.es

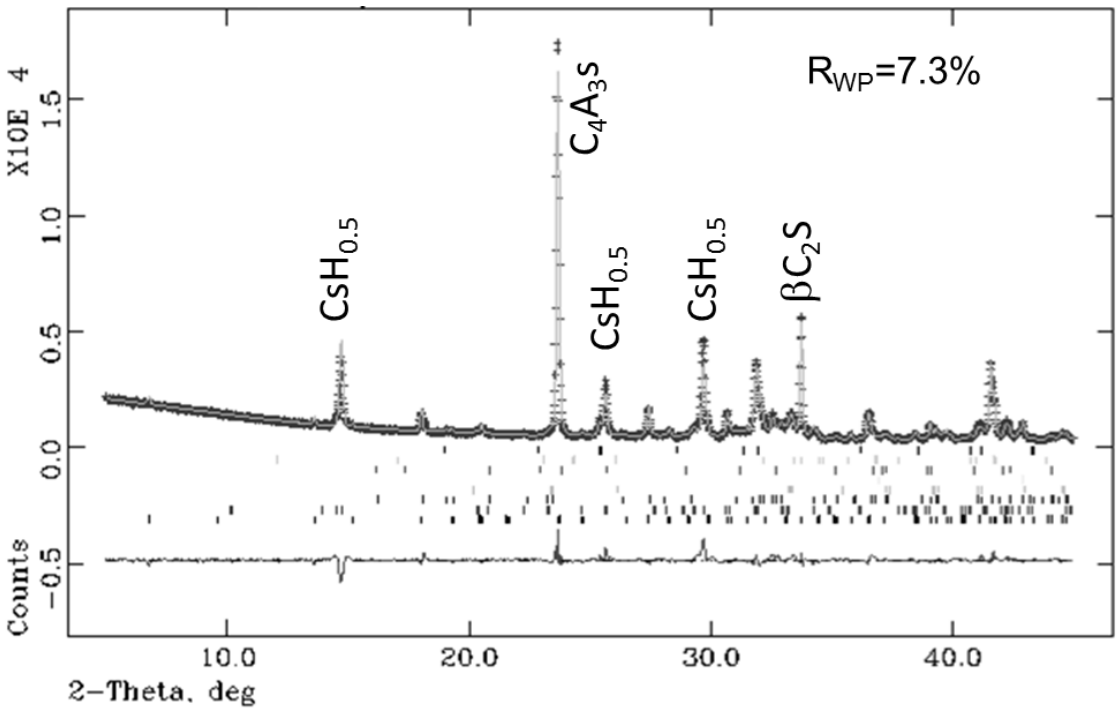

Fig. S1. Rietveld LXRPD plot (λ=1.54 Å) for the anhydrous cement.

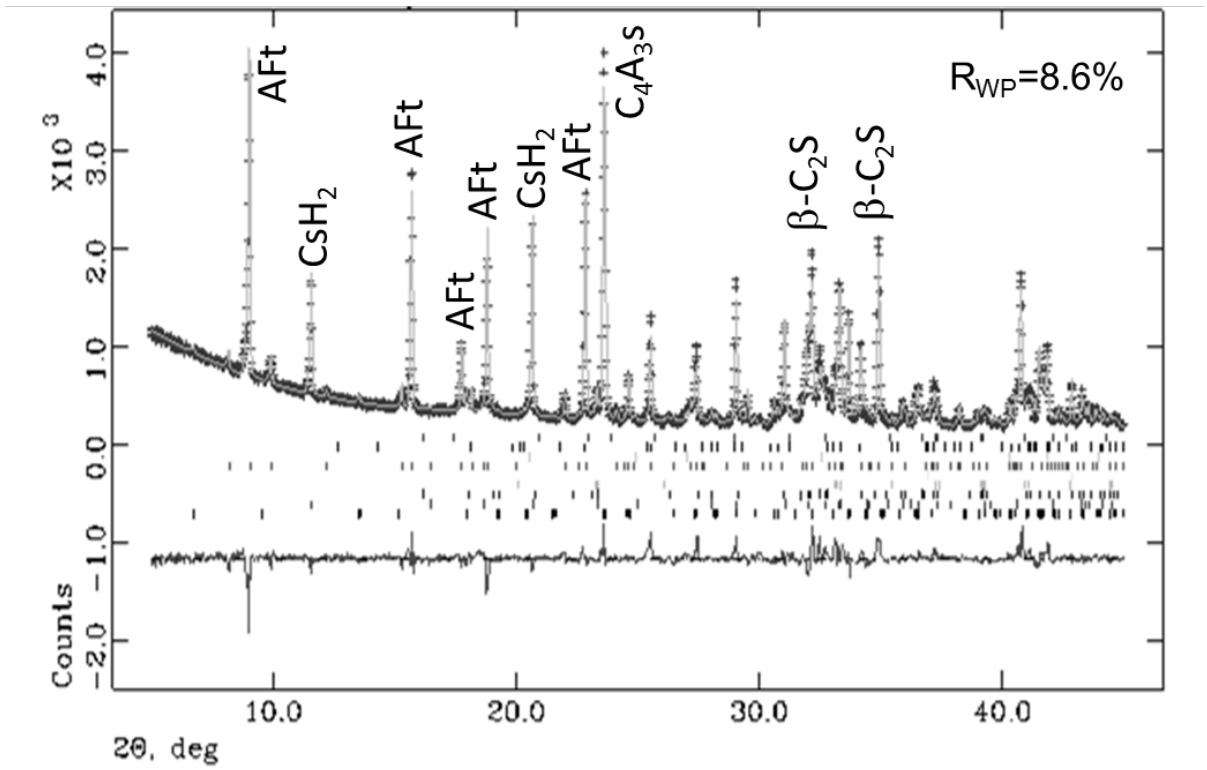

Fig. S2. Rietveld LXRPD plot (λ=1.54 Å) for the paste prepared with 0.10 wt% of polycarboxylate at 1 day.

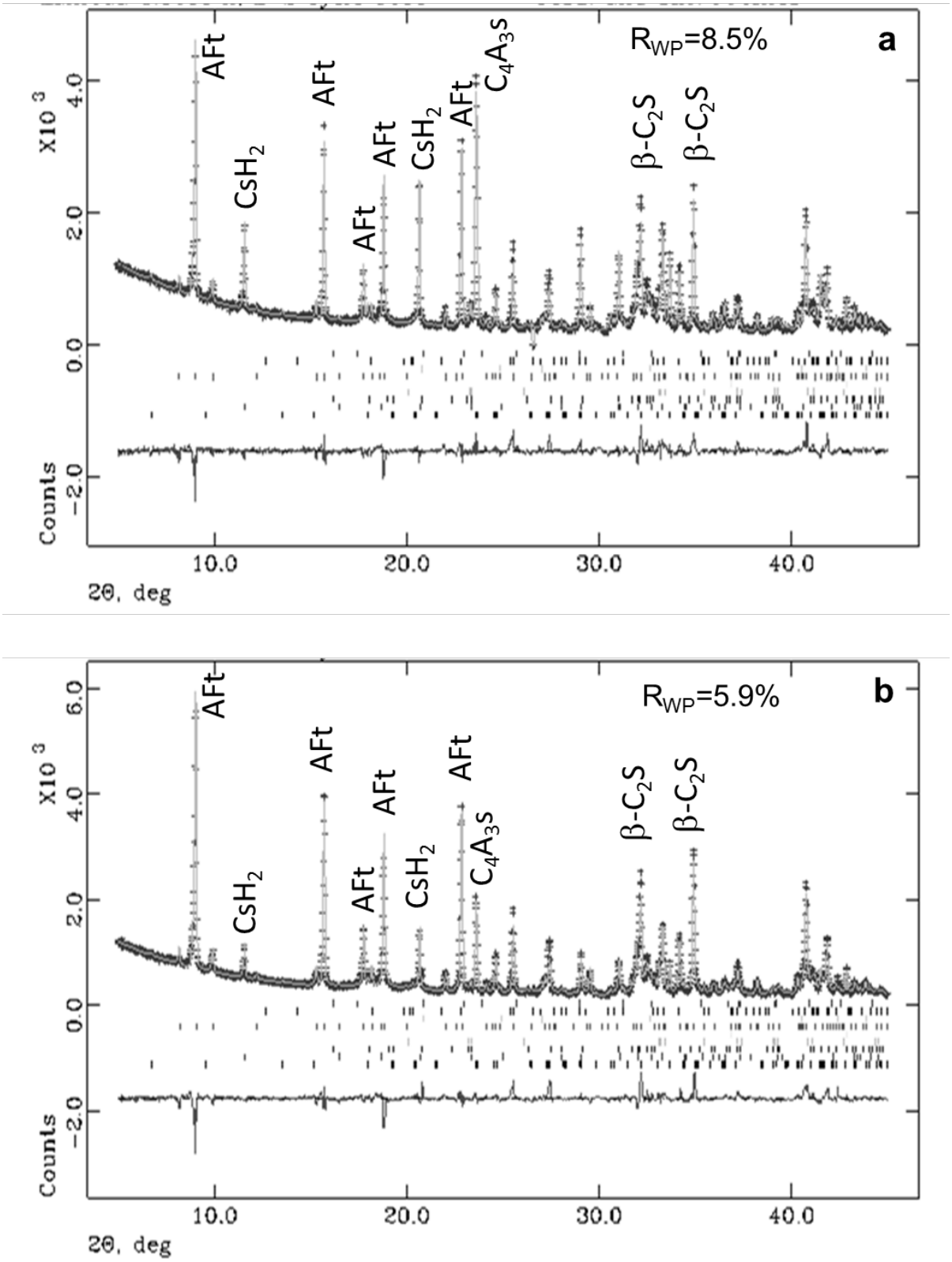

Fig. S3. Rietveld LXRPD plot (λ=1.54 Å) for the paste prepared with 0.15 wt% of tartaric acid at 1 day (a), and 7 days (b) of hydration.

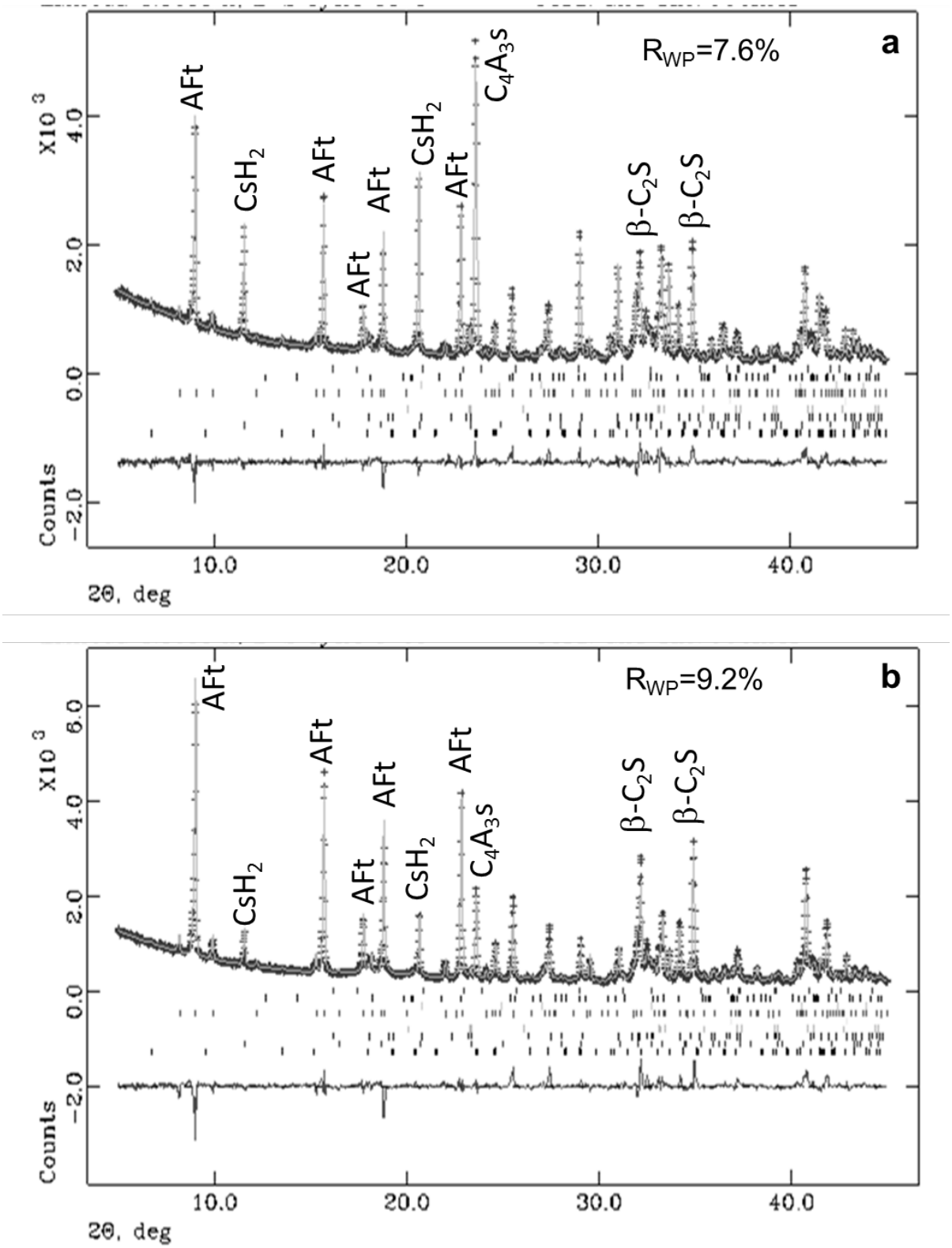

Fig. S4. Rietveld LXRPD plot (λ=1.54 Å) for the paste prepared with 0.30 wt% of phosphonic acid at 1 day (a), and 7 days (b) of hydration.

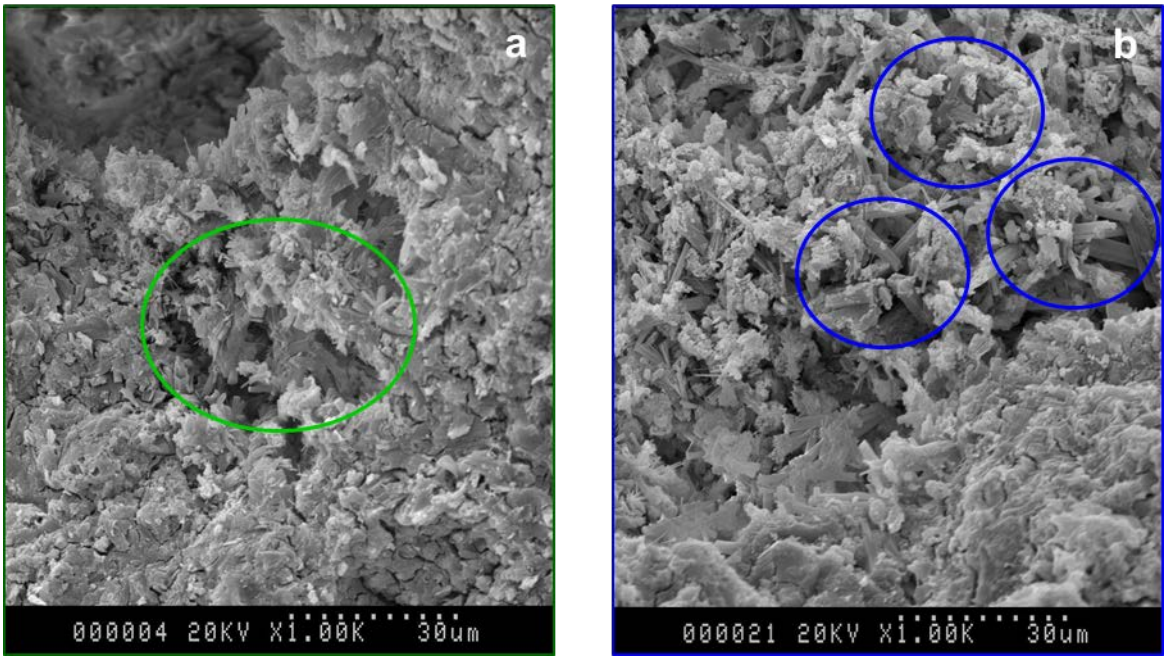

Fig. S5. SEM micrographs of fracture surfaces of PC (a) and PA (b) pastes at 1 day of hydration.

Table S1. X-ray fluorescence analysis for both raw materials (CSA clinker and gypsum).

	CSA (wt%)	Gypsum (wt%)
CaO	41.97	31.20
Al_2O_3	33.80	0.37
SO_3	8.80	42.40
Fe_2O_3	2.37	0.12
SiO_2	8.20	0.73
MgO	2.73	0.10
K_2O	0.25	0.05
TiO_2	1.50	-
SrO	0.15	2.38
P_2O_5	0.13	0.44
ZrO_2	0.07	-
Na_2O	<0.08	0.20
LoI	-	22.00